ISSN: 2977-683X

Research Article

Journal of Metabolic and Diabetes Research

Immunoprofiling of Alcohol-Activated Hepatic Stellate Cells Reveals Mechanisms of Immune Evasion Through NK/T Lymphocyte Checkpoint Signaling

Alexander Kessler[1], Peiyin Ho[1], Yibu Chen[2], Subarna Biswas[3] and Douglas E Feldman[1*]

[1]Department of Pathology, University of Southern California, Keck School of Medicine of USC, Angeles, CA 90033, USA
[2]Bioinformatics Service, Department of Health Sciences Libraries, Keck School of Medicine, Los Angeles, CA 90033, USA
[3]Department of Surgery, University of Southern California, Keck School of Medicine, Los Angeles, CA 90033, USA

[*]Corresponding author
Douglas E. Feldman, University of Southern California, Department of Pathology, Keck School of Medicine of USC, Angeles, CA 90033, USA.

Received: July 29, 2025; **Accepted:** August 04, 2025; **Published:** August 12, 2025

ABSTRACT

Background: Chronic heavy alcohol consumption induces the pathogenic activation of hepatic stellate cells (HSC) and their conversion into myofibroblasts (Myo), which together comprise a central disease hub. Clinical successes of immunotherapy in targeting pre-specified cell populations has suggested the possibility of harnessing the immune system to target and eliminate aHSC/Myo, however aHSC evade immune surveillance through mechanisms that remain poorly understood.

Methods: We utilized a combination of FACS profiling of HSC surface-expressed immunomodulatory ligands, in vitro cytotoxicity assays, and scRNA-seq profiling of liver non-parenchymal cells to assess the impact of immunotherapy on HSC/Myo and immune cell populations.

Results: In a mouse model of alcohol-induced liver damage, blocking CTLA-4, TIGIT, and PD-1 checkpoints enhanced immune targeting of hepatic cells. However, this did not reduce fibrosis or improve liver function. Single-cell analysis showed the treatment increased hepatic infiltration of NK and T cells while decreasing immunosuppressive Treg. However, engagement of PD-1 and TIGIT checkpoints also failed to ameliorate fibrosis or liver function. These findings suggest that while combined checkpoint blockade alters the hepatic immune landscape, it is insufficient as a standalone therapy to reverse alcohol-related liver fibrosis.

Conclusions: Immunotherapeutic modalities that enable precision targeting of HSC/Myo may be necessary to achieve therapeutic gains.

Introduction

Alcohol-associated liver disease (AALD) accounts for nearly half of all cirrhosis cases in the United States and represents a major public health problem and economic burden worldwide [11-16]. AALD is manifested as a spectrum of clinical disorders ranging from steatosis (fatty liver) to alcohol-associated steatohepatitis (ASH), a combination of steatosis and inflammation. While ASH is reversible, if untreated it may progress to cirrhosis and hepatocellular carcinoma. ASH is associated with high rates of mortality: up to 40% of severe ASH patients die within six months of clinical diagnosis [17,18]. Currently there are no FDA-approved therapies for AALD, underscoring the urgent need for deeper disease understanding and the approval of new treatments.

Hepatic stellate cells (HSC) are central mediators of AALD onset, progression, and severity. Following long-term heavy alcohol consumption, quiescent HSC (qHSC) activate and transdifferentiate into myofibroblast-like (Myo) cells, which secrete collagen and other extracellular matrix components and

Citation: Alexander Kessler, Peiyin Ho, Yibu Chen, Subarna Biswas, Douglas E Feldman. Immunoprofiling of Alcohol-Activated Hepatic Stellate Cells Reveals Mechanisms of Immune Evasion Through NK/T Lymphocyte Checkpoint Signaling. J Metab Diabet Res. 2025. 2(2): 1-10.
DOI: doi.org/10.61440/JMDR.2025.v2.09

promote liver inflammation through the release of inflammatory cytokines, contributing to liver injury [3,4,19,20]. These observations have led to the proposal that selective elimination of aHSC may offer a therapeutic benefit.

Harnessing the innate immune system, in particular natural killer (NK) cells, may represent a promising strategy to selectively target and eliminate aHSC. The conversion of quiescent HSC to aHSC is accompanied by a transient increase in expression of NK cell activating ligand retinoic acid inducible gene 1 (RAE1), which corresponds with vulnerability of early-activated HSC to NK cell killing. In contrast, chronically activated HSCs lose their cytoplasmic stores of retinol and do not produce RA and RAE1, impairing NK cell cytotoxicity against HSC [6,7,21,22]. Chronic alcohol consumption also impairs the immune surveillance and cytotoxicity of NK cells by arresting NK cell development at the CD27+CD11b+stage [23,24]. Alcohol-induced downregulation of NKG2D, TRAIL, and interferon- (IFN-) y expression has also been detected on NK cells and is associated with the activation of hepatic stellate cells [25].

Intriguingly, knockdown of the NK cell inhibitory receptor iKIR stimulates NK targeting of activated HSC [5], highlighting the potential for harnessing the immune system to target and eliminate aHSC/Myo. However, the mechanisms underlying immune evasion by HSC remain incompletely understood, limiting therapeutic development.

In this study, we profiled the expression of a panel of immune-modulating ligands expressed by HSC, and show that CD80, a key immune checkpoint ligand, is dynamically expressed during HSC activation. While antibody blockade of the CD80/CTLA-4 checkpoint facilitates aHSC targeting by CD8+ T cells in vitro, combined blockade of CTLA-4, TIGOT, and PD-1 checkpoints does not lead to resolution of alcohol-induced liver fibrosis or amelioration of liver function. Using single-cell RNA-seq profiling, we show that checkpoint blockade reduces the burden aHSC, but expands activation of Th17 T-cells and increases hepatic infiltration of inflammation-promoting immune subsets. Furthermore, the inverse therapeutic approach-- immune suppression via combination engagement of the TIGIT/PD-1 checkpoints—likewise fails to reduce fibrosis or restore liver function. These observations highlight the nuanced and multifaceted role of the immune system in AALD, and suggest that highly selective targeting of aHSC/Myo may be necessary to achieve significant amelioration of liver function.

Materials and Methods

Flow Cytometry Analysis

Mouse HSC were isolated from liver tissue using standard protocols [69], followed by staining with fluorescently labeled antibodies specific for individual checkpoint ligands. The following antibodies were used: CD155-FITC (ThermoFisher #2H7CD155), CD274_PD-L1-AIexa 488 (ThermoFisher 53-5983-42), and CD80-PE (clone 2D10.4, # 12-0809-42). FACS was performed using a BD FACSAria III. HSC were also measured for UV autofluorescence at 328 nm.

Cytotoxicity Assay

Individual groups of NK cells or CD8+ T cells were cultivated for 6 h with HSC target cells in the absence or presence of anti-CTLA-4 blocking antisera or isotype-matched control IgG (15 ug/ml). Cells were then harvested and dyed with propidium iodide PI (Sigma-Aldrich, USA), a dye that only enters cells with compromised membranes. The percentages of PI+ cells in each group were measured with flow cytometry.

Alcohol and Hfd Mouse Model

Male or female B6 mice (8 wk old) were fed ad libitum for 2 weeks with a liquid diet containing two different levels of cholesterol and saturated fat: 2.32g/L cholesterol and 23.2g/L lard (DYET#710142) or 46% reduced cholesterol and lard content (#710383). The diet is then switched to those containing ethanol (#710362 or #710384) for ethanol-fed mice. Ethanol content is gradually increased from 1% (v/v) on day 1 to 4.35% (v/v) on day 12 until the end of feeding. If additional alcohol binge is required, a weekly binge of alcohol is given from the second week of ethanol feeding, via a stomach tube at the initial dose of 3.5g/kg which is gradually increased to 4.5g/kg. For control mice, isocaloric dextrose solution is given as a binge.

In Vivo Checkpoint Modulation

For ICB treatments, mice were administered a cocktail of blocking antisera for CTLA-4 (Novus Biologicals #1003705, 25 ug), TIGIT (Invivogen mab10-010, 40 ug), and PD-1 (invivogen mpd1-mab-15-50, 25 ug), or isotype-matched non-specific control IgG (BioXCeII #BE0083), infused biweekly into mice in each of the alcohol or control feeding arms via i.p. injection, commencing at week 3 of each diet regimen. For the reciprocal series of in vivo checkpoint agonist experiments, mice were administered antisera specific for TIGIT (BioXCeII mid/VOMAb #BE0274, 30 ug) and recombinant PD-L1 extracellular domain (Sino Biological #50010-M08H, 40 ug).

Immunohistochemistry and Immunofluorescence

Formalin-fixed liver tissue sections were stained with H&E for histological analysis or Sirius Red for collagen deposition. Sections were separately stained for CD69 using CD69 Monoclonal Antibody (H1.2F3), Biotin, eBioscience™, followed by streptavidin-HRP (Invitrogen S911). Slides were imaged using a ZeissAxioScan.z1 microscope and images analyzed using Zeiss Zen 3.9 software. The collagen area/portal vein area were quantified by digital imaging with National Institutes of Health Scion Image and Adobe Photoshop (San Jose, CA).

Serum and Liver Analysis

Serum was analyzed for alanine aminotransferase (ALT) and aspartate aminotransferase (AST) by blood chemistry panel (Antech Diagnostics, Inc) to assess liver function. Liver tissue was used for RNA and protein expression studies.

Scrna-Seq Library Preparation

All samples were processed using the Parse Biosciences Evercode WT Mini v2 kit. NPC were isolated from mouse treatment cohorts. Single cell suspensions were counted and centrifuged at 200 g for 5 minutes at 4 °C. Pellets were resuspended in lysis buffer (250 mM sucrose, 25 mM KCI, 5 mM MgCI2, 10mM Tris pH 8.0, 225 1mM DTT, 0.2 U/mL RNasin (Promega #N2511), 0.005 U/mL DNase I (Thermo Fisher 226 Scientific # EN0521), 0.1% Triton X-100, sterile H2O). Extraction of nuclei was confirmed using the SYTOX Green nuclear stain (Thermo Fisher

Scientific # S7020), with 100% efficiency across all lines. Nuclei were input into the Parse Biosciences Evercode Fixation Kit as per manufacturer instructions. Individual sub-libraries composed of 10,000 nuclei each and sequenced targeting 20,000 reads per nuclei (as per manufacturers protocol). Resultant FASTQ files were processed using the Parse Biosciences provided split-pipe 1.2.1 software package to perform alignment to the hg38 genome, and subsequent unique molecular identifier (UMI) counts with sample barcode demultiplexing. Individual sub-libraries were processed separately before being merged. CellBender 0.3.2 30 was also used to test for doublets in the dataset. Mitochondrial expression and number of features identified for each nucleus was calculated using Seurat 5.1.

Scrna-Seq Data Analysis

The single cell RNA-seq dataset was processed, explored and visualized using TrailmakerTM (https://app.traiImaker.parsebiosciences.com/; Parse Biosciences, 2024). Unfiltered count matrices were uploaded to Trailmaker, and dead or dying cells were removed by filtering droplets with high mitochondrial content. Outliers in the distribution of number of genes vs number of transcripts were removed by fitting a linear regression model. Cells with a high probability of being doublets were filtered out using the scDblFinder method. Data normalization, principal-component analysis (PCA) and data integration using Harmony were performed on data from high-quality cells. Clusters were identified using the Leiden method, and a Uniform Manifold Approximation and Projection (UMAP) embedding was calculated to visualize the results. Cluster-specific marker genes were identified by comparing cells of each cluster to all other cells using the presto package implementation of the Wilcoxon rank-sum test.

Statistical Analysis

All experiments were repeated at least three times. Data are reported as mean + s.d. unless otherwise stated. Analyses for statistical significance were performed in GraphPad Prism 6 (GraphPad Software, Inc., La Jolla, CA, USA) and Microsoft Excel using Student's t-test, one-way ANOVA with Tukey's multiple comparisons test, Chi-square analysis and Fisher's exact test as appropriate. Images represent typical experimental results.

Results

To gain additional insight into immune modulation by HSC, we profiled the expression of immune checkpoint ligands by HSC through a range of activation states, from freshly isolated, qHSC to late-activated (day 14) aHSC. Our analysis revealed that CD80, a high-affinity ligand of the CTLA-4 checkpoint receptor, is dynamically expressed on both qHSC and late-activated HSC, while levels transiently decrease in early-activated (day 5) HSC (Figure 1A). In contrast, the checkpoint ligands PD-L1 and CD15 were not expressed above background levels in aHSC (Figure S1). lmmunoblotting of a membrane-enriched HSC fraction using anti-CD80 antisera confirmed a dynamic increase in CD80 expression during HSC activation (Figure 1B). CTLA-4 competes with the CD28 activating receptor for binding of B7 ligands such as CD80, and increased CTLA-4: B7 binding transmits a net negative signal, limiting IL-2 production, and diminishing T cell proliferation and survival [26,27]. These findings therefore suggest a potential role for the CD80/CTLA-4 checkpoint in evasion of lymphocyte surveillance and targeting.

To test this experimentally, we performed in vitro cytotoxicity assays in which HSC at different stages of activation were co-incubated with CD8+T effector cells, in the presence of either CTLA-4 blocking antisera or isotype-matched control antisera. At both tested HSC: T cell ratios, addition of CTLA-4 blockade enhanced CD8+ T destruction of activated (day 14) HSC, but did not affect T cell targeting of HSC at an early-intermediate activation state (day 5) (Figure 1C).

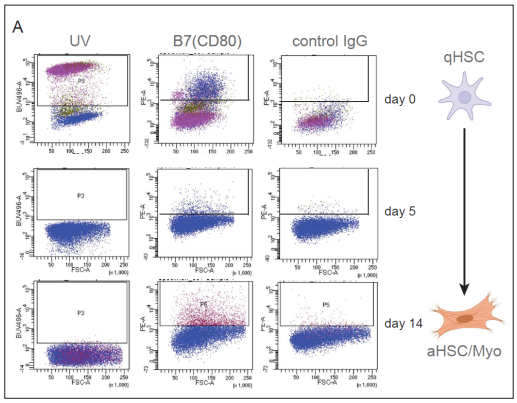

Figure 1A: A. FACS profiling of murine HSC showing dynamic expression of lymphocyte checkpoint ligand B7 (CD80) following culture in vitro for the indicated times.

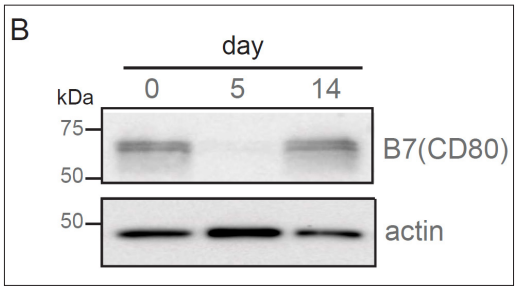

Figure 1B: Western immunoblot of B7 (CD80) in membrane-enriched subcellular fraction.

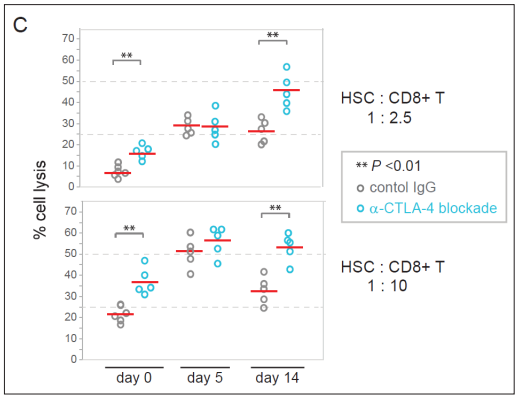

Figure 1C: In vitro cytotoxicity assay showing lysis of HSC following co-culture with purified CD8+ T cells (2.5:1 T:HSC) [7].

Figure 1: Dynamic expression of B7 (CD80) during HSC activation.

Given this increase in aHSC targeting following exposure to combination checkpoint blockade, we next sought to evaluate

the impact of CTLA-4 blockade on liver function and fibrosis in a mouse model of acute-on-chronic AALD, utilizing an alcohol feeding regimen that closely recapitulates key aspects of clinical AALD [28,29]. Given that CD28 is co-regulated by the PD-1 checkpoint [30], and that the mechanistic convergence of the TIGIT and PD-1 inhibitory pathways necessitates co-blockade to optimize lymphocyte responses [31], we pursued the combined antibody blockade of CTLA-4/TIGIT/PD-1 checkpoints to maximize therapeutic potential.

Mice were allowed ad lib consumption of a high-cholesterol, high-fat liquid diet (HCFD) containing either isocalorically substituted maltose-dextrins or 4.0% ethanol for 10 weeks. A binge bolus dose (4g/kg) of ethanol was given weekly from the second week during the feeding (Figure 2A). This weekly ad lib HCFD+AIc+Binge model robustly induces increased plasma ALT, hepatitis with monocyte infiltration in ”50% of the mice after 8 weeks, and activation of HSC and pericellular and perisinusoidal liver fibrosis [32]. Mice were dosed twice weekly for six weeks with combined CTLA-4/ TIGIT/PD-1 blockade or i=non-targeting control antisera, and liver function was then monitored by measurement of serum ALT/AST, and by Sirius Red fibrosis staining of sectioned liver tissues recovered at the experimental endpoint.

We observed marked elevations of plasma AST and ALT in alcohol-fed mice (Figure 2B), as expected in this acute-on-chronic model of alcohol consumption [32,33]. Immune checkpoint blockade (ICB) treatment, however, did not reduce levels of serum AST or ALT (Figure 2B). Furthermore, Sirius Red staining revealed modestly increased fibrosis levels in the checkpoint blockade cohort, though the measured increase did not achieve statistical significance (Figure 2C, D), while promoting infiltration of activated, CD69+ NK and T lymphocytes, as determined by immunohistochemistry (Figure S2). Collectively, these observations indicate that combination immune checkpoint therapy does not confer a therapeutic benefit in the setting of acute-on-chronic alcohol consumption, and may deepen the severity of liver injury.

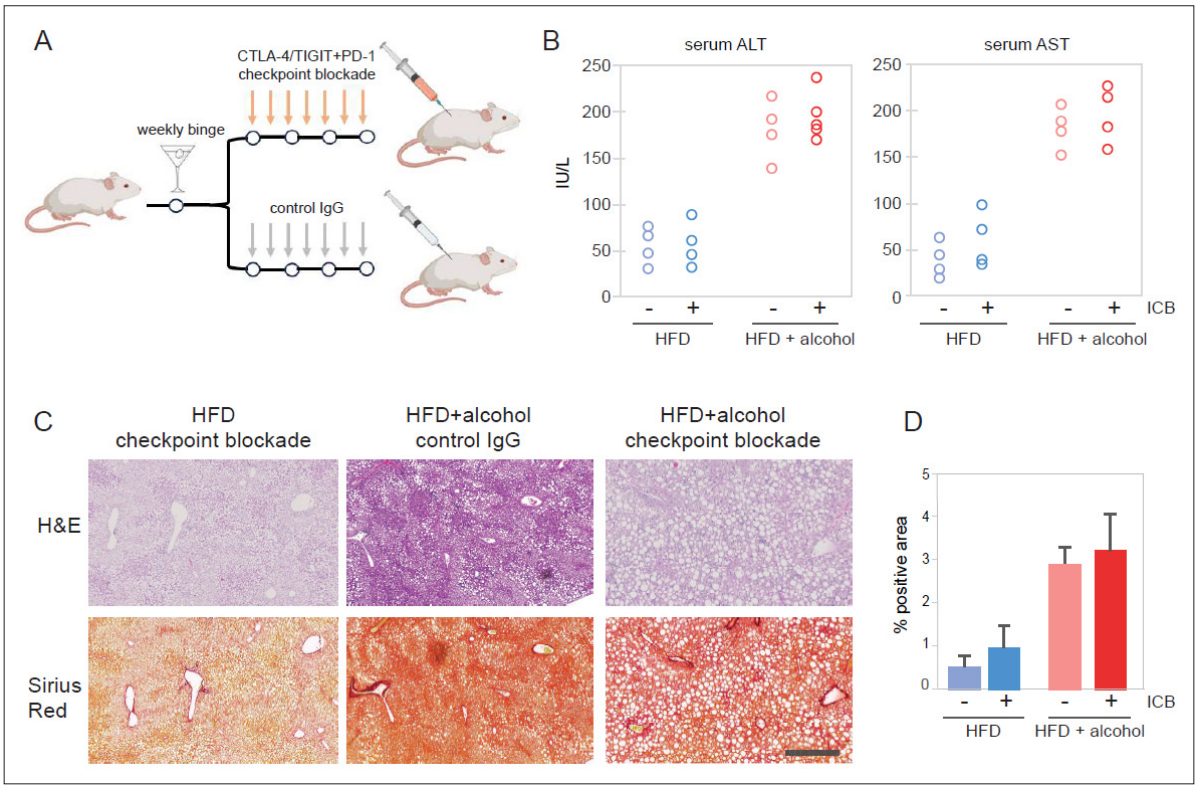

Figure 2: Effect of CTLA-4/TIGIT blockade on alcohol-promoted liver fibrosis.

Figure 2A: Schematic of acute-on-chronic mouse model of AALD. Mice were allowed ad lib consumption of a high-cholesterol, high-fat liquid diet (HCFD) containing either isocalorically substituted maltose-dextrins or 4.0% ethanol for 10 weeks. A binge bolus dose (4g/kg) of ethanol was given weekly from the second week during the feeding. This weekly ad lib HCFD+AIc+Binge model robustly induces increased plasma ALT, hepatitis with monocyte infiltration in -50% of the mice after 8 weeks, and activation of HSC and pericellular and perisinusoidal liver fibrosis

Figure 2B: Serum ALT and AST levels at necropsy. Immune checkpoint blockade combination therapy (CTLA-4/TIGIT/PD-1) did not lead to a reduction in liver enzymes.

Figure 2C: H&E and Sirius Red staining of mouse livers following treatment with the indicated control or immune checkpoint-blocking antibodies. Scale bar, 50 km.

Figure 2D: Quantification of Sirius Red staining in mouse livers following the indicated treatments [19].

To better understand how immune checkpoint blockade impacts the liver non-parenchymal cell (NPC) landscape in the setting of acute-on-chronic alcohol consumption, we performed droplet-free single cell RNA sequencing (scRNA-seq) analysis of NPC isolated from dissociated mouse livers (n=2 mice per condition). We obtained 43,647 single-cell transcriptomes (225 median transcripts/cell), enabling high-definition cell subtype profiling and the comparison of NPC following acute-on-chronic alcohol feeding and following treatment with the immune checkpoint blockade (Figure 3A, B). We applied strict filtering on data, including expressed genes and unique molecular identifiers (UMIs), and performed additional signal normalization and scaling using strict statistical cutoffs.

We first evaluated how treatment with immune checkpoint blockade impacted the conversion of Qhsc into aHSC and subsequently to collagen-secreting Myo. Pseudotime studies characterizing cell developmental programs based on transcriptional similarities have suggested a cell trans-differentiation trajectory from HSC into Myo, with each cell type composed of four distinct subclusters [34-36]. Treatment with ICB led to a reduction in the relative abundance of late-activated HSC3 and HSC4 clusters, together with a concomitant depletion of late-stage myofibroblast subpopulations, including Myo III (Egr1, KIf2) and Myo IV (Fb/nJ, Meg3) (Figure 3C-E).

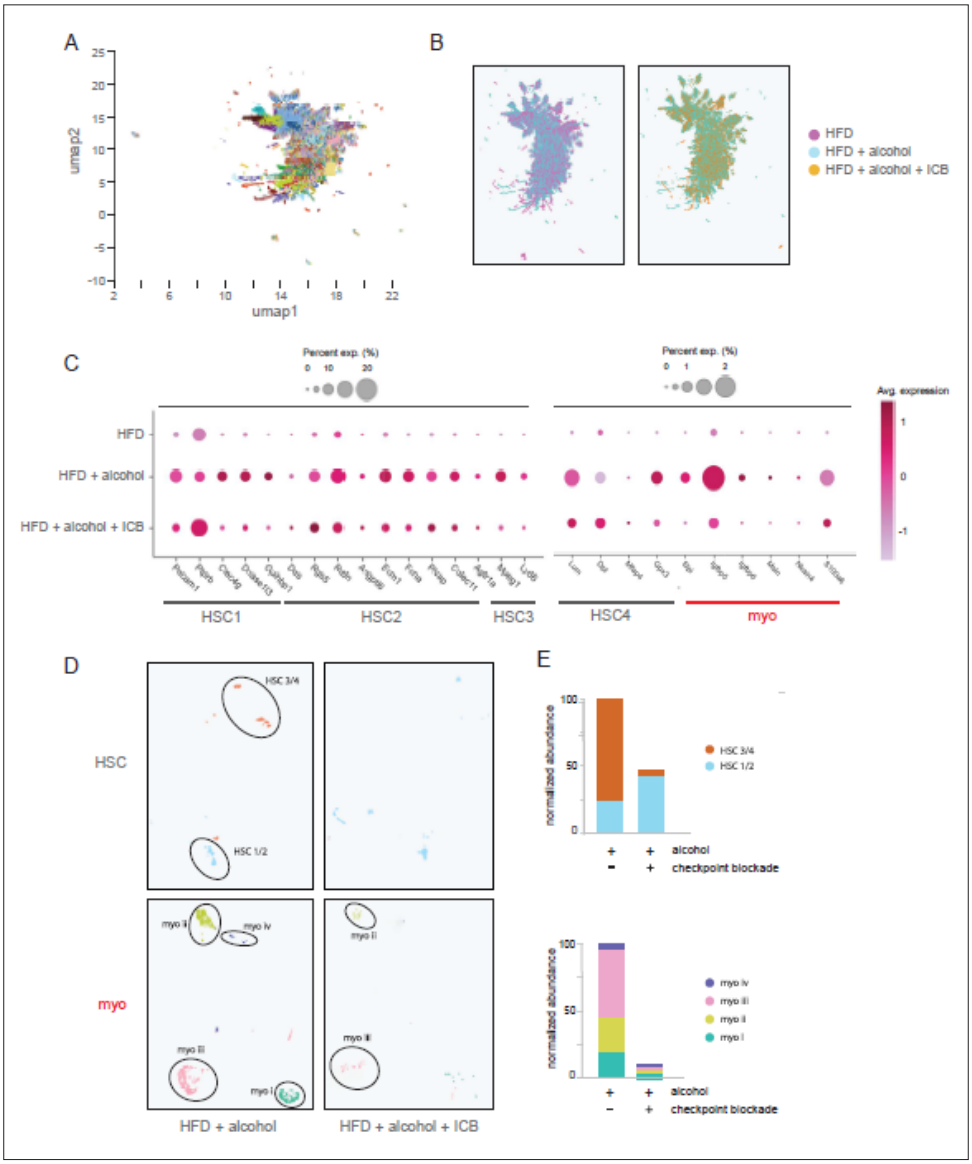

Figure 3: Blockade of the CTLA-4/TIGIT co-inhibitory axis induces elimination of aHSC/Myo.

Figure 3A: scRNA-seq profiling of mouse liver non-parenchymal cells following treatment with ICB of CTLA-4/TIGIT/PD-1 showing total cell subclusters.

Figure 3B: Comparative representation of cell subclusters following high-fat diet (HFD) and alcohol-feeding with checkpoint blockade or control IgG treatment regimens.

Figure 3C: Depletion of aHSC and Myo gene expression signatures following immune checkpoint blockade therapy. The size of dots indicates percentage of expressed cells and the color indicates average scaled expression level.

Figure 3D: Cluster analysis showing loss of aHSC and Myo subpopulations following immune checkpoint blockade therapy.

Figure 3E: Relative abundance of HSC subclusters in the absence or presence of immune checkpoint blockade.

Figure 3F: Depletion of Myo subclusters following ICB treatment [29].

Given the reduced representation of alcohol-activated HSC and late-stage Myo subpopulations without a corresponding reduction in fibrosis or improvement in liver function, we next sought to profile changes in the liver immune landscape following ICB treatment. NK and T cells serve as major effectors of ICB treatment, and are each composed of multiple cellular subtypes that can either promote or suppress activating and inflammatory responses [39-41]. We therefore compared differences in relative representation of T cell subclusters, annotated through the expression of canonical marker genes associated with the expression of known cell population-specific transcript signatures. In particular, we found that ICB increased the abundance of activated (IFN-gamma, T-bet, CXCR3, CCR5) CD8+ T cells [42], as well as pro-fibrotic Th1 and Th17 (IL-17R, CCR6+) T cells (Figure 4A). In contrast, cell clustering analysis revealed suppression of quiescent (CD27+, CD45+) CD8+ T cells, along with a near-complete loss of CD25+ FoxP3+ Treg (Figure 4A). This analysis additionally revealed elevated expression of T cell activation markers (Tnf, Gzmb, CD69) and diminished levels of inhibitory genes (CD244, GITR/AITR) in response to ICB treatment (Figure 4B).

Concomitant with these changes, scRNA-seq profiling revealed increased infiltration of monocytes and monocyte-derived macrophages (Mo/MoMF), including M1 polarized and Ly-6C+ macrophages, which favor Th1 proinflammatory responses and are associated with perisinusoidal and pericellular liver fibrosis, and severe ASH [43, 44] (Figure 4C). Relative expression levels for selected cell lineage marker genes for these subtypes are shown in Figure 4D. In agreement with previous reports demonstrating cross-communication between activated HSC and KC [37,38], ICB treatment also diminished expression of genes associated with activated Kupffer cell subsets, including the KC2 marker Bmp2, and the KC3 markers Nr2f2 and Kdr (Figure 4E). Thus, while ICB diminishes fibrosis-inducing, late-stage aHSC and Myo, this effect may be offset by increased infiltration and activation of pro-inflammatory hepatic NK and T cell and macrophage subpopulations.

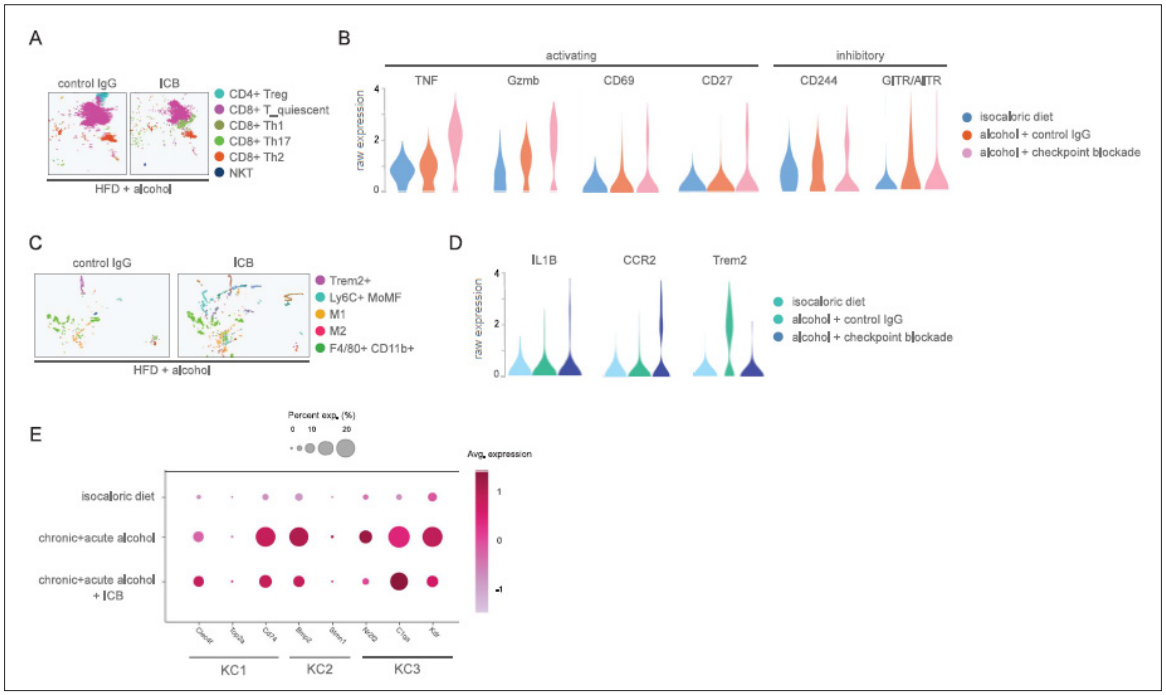

Figure 4: Impact of CTLA-4/TIGIT blockade on hepatic NK and T lymphocyte subsets.

Figure 4A: scRNA-seq clustering of mouse NK/T/NKT cell populations following treatment with ICB or control antisera.
Figure 4B: Violin plots showing expression levels of genes implicated in T cell activation or dormancy. Representation of differential cell clustering following the indicated alcohol-feeding and treatment regimens. showing expression levels in macrophage clusters for genes implicated in pro-inflammatory responses (TNF, Gzmb, CD69, CD27) or suppressive responses (CD244, GITR/AITR).
Figure 4C: scRNA-seq clustering of mouse macrophage populations following the indicated treatments. Application of ICB therapy leads to increases in M1 and Ly6C+ MoMF subpopulations, and correspond to increased liver injury.
Figure 4D: Violin plots showing expression levels in macrophage clusters for genes implicated in pro-inflammatory responses (IIIB, Ccr2) or suppressive responses (Trem2).
Figure 4E: Dynamic changes in Kupffer cell gene expression signatures following immune checkpoint blockade therapy. The size of dots indicates percentage of expressed cells and the color indicates average scaled expression level [42].

We therefore sought to determine whether the inverse strategy- immune suppression through checkpoint engagement- could reduce liver fibrosis and restore liver function. Mice were administered a TIGIT/PD-1 checkpoint agonist cocktail designed to broadly suppress NK and T lymphocyte activity (Figure5A). However, combination engagement of these checkpoints failed to decrease serum ALT/AST levels (Figure 5B) and did not result in a significant reduction in alcohol-promoted liver fibrosis or steatosis, as determined by histological analysis of mouse liver tissues (Figure 5C, D). We conclude that immune checkpoint engagement does not yield significant restoration of liver function in the setting of alcohol-promoted fibrosis and tissue injury.

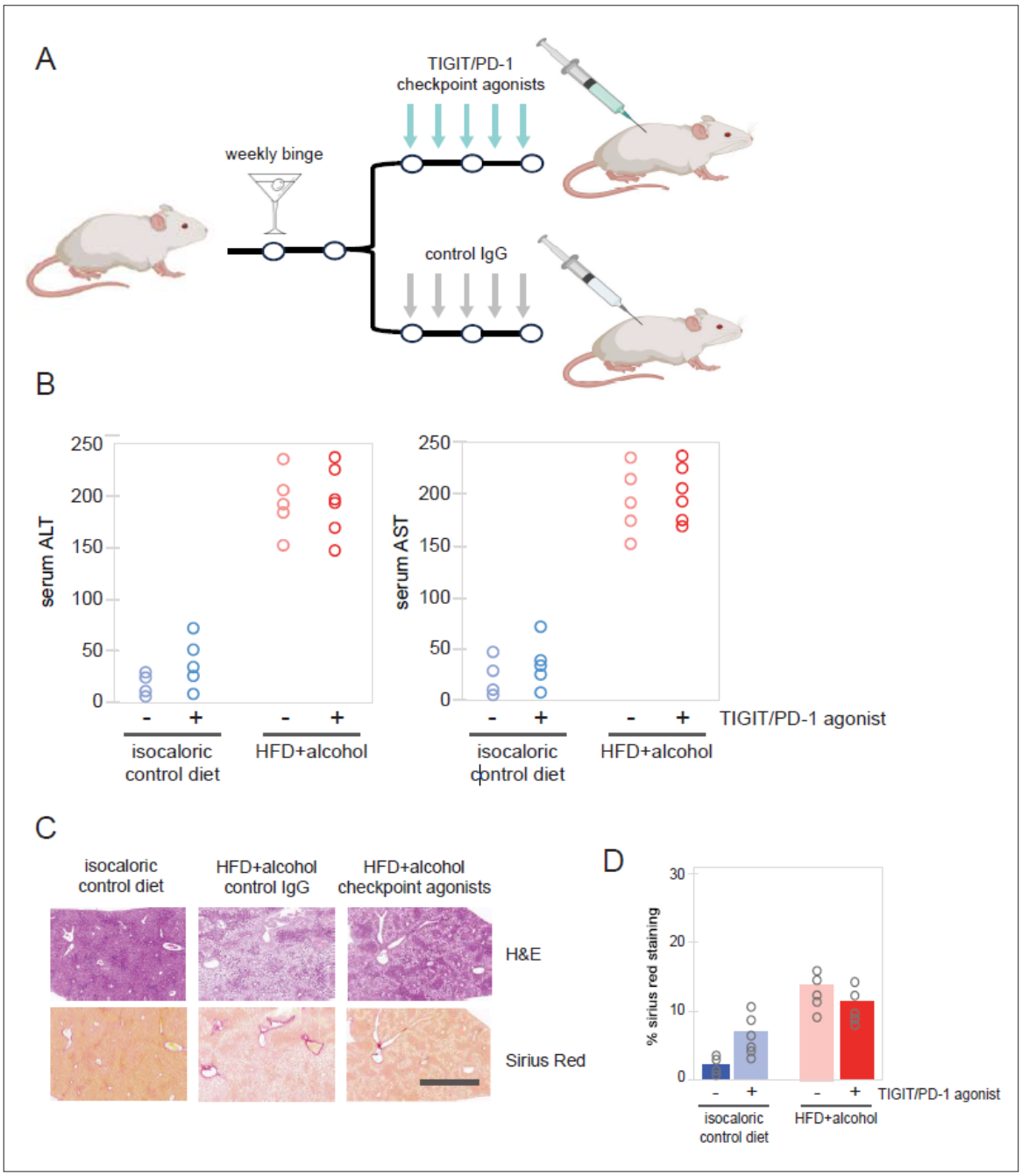

Figure 5: Effect of TIGIT/PD-1 checkpoint engagement on liver function.

Figure 5A: Schematic of acute-on-chronic mouse model of AALD and checkpoint agonist dosing.
Figure 5B: Serum ALT and AST levels at necropsy showing that administration of combined TIGIT/PD-1 checkpoint agonists did not lead to a reduction in liver enzymes.
Figure 5C: H&E (upper panels) and Sirius Red fibrosis staining (lower panels) of mouse livers following treatment with the indicated control or immune checkpoint-agonist antibodies. Scale bar, 50 pm.
Figure 5D: Quantification of Sirius Red staining in mouse livers following the indicated treatments.

Discussion

Elimination of aHSC/Myo mitigates liver damage resulting from chronic alcohol consumption, and represents a therapeutic objective for the treatment of AALD [2,4,5,19,45,46]. The recent clinical success of immunotherapy in selectively targeting pre-specified cell populations [47-49] has suggested the utility of this approach for the treatment of AALD. Here, we show that aHSC can evade immune surveillance through surface expression of the B7/CD80 immunomodulatory ligand, and that combined blockade of the CTLA-4/TIGIT/PD-1 checkpoints stimulates lymphocyte targeting of aHSC/Myo. However, this approach fails to diminish fibrosis or ameliorate liver function, underscoring the multifaceted complexity of the hepatic immune response in AALD.

Alcohol-promoted immune dysfunction is manifested through suppression of NK and T lymphocyte surveillance , as well as hepatic infiltration of pro-inflammatory monocytes, macrophages and effector T cells which together drive fibrosis and tissue injury. Our findings reveal that combined blockade of the CTLA-4/TIGIT/PD-1 axis stimulates targeting of distinct aHSC subtypes (HSC2-4), while also diminishing hepatic Treg, which may contribute to hepatic injury [50,51]. However, by inhibiting profibrotic Th17 and CD8+ T cells, Foxp3+ Treg cells may also help to maintain immune homeostasis [52,53]. Treg cells can also suppress the activation of Th2 cells and infiltrating Ly-6Ch'^hCCR2h'^h monocytes/macrophages, reducing chronic inflammation and attenuating hepatic fibrosis [54,55]. Thus, checkpoint blockade may drive an imbalance of Th17/Treg, leading to excess immune activation, offsetting the potential therapeutic benefit of eliminating aHSC/Myo [52,56].

Interestingly, our findings reveal that the inverse strategy—immune suppression via engagement of the TIGIT/PD-1 checkpoints—likewise fails to confer a significant therapeutic benefit. These observations are consistent with reports demonstrating activation of multiple types of immune cells--T cells, NKT cells, Kupffer cells, and mucosal-associated invariant T cells-- in the setting of alcohol-induced liver injury. For instance, Koda and colleagues demonstrated a direct role for CD8+ tissue-resident memory CD8+ T (CD8+ Trm) cells in resolving liver fibrosis, and found that a reduction of liver CD8+ Trm cells, maintained by tissue IL-15, significantly delayed fibrosis resolution, while adoptive transfer of these cells protected mice from fibrosis progression [57]. Similarly, AALD patients exhibit impaired innate adaptive responses, lymphocyte depletion, and increased expression of T cell exhaustion markers [58,59].

Collectively, our data suggest that precision targeting of aHSC/Myo, rather than one-dimensional activation or blockade of checkpoints, may offer a greater therapeutic index. Recent clinical advances in targeting pre-defined cell populations using bi-specific T cell engagers [60-63], as well as the development of engineered NK and T cells expressing target-selective chimeric antigen receptors (CAR) [47,61,64-67], highlight the potential of these emerging platforms for selective targeting of the aHSC/Myo disease hub. Recent single-cell transcriptome analysis of HSC/Myo have uncovered surface antigens expressed by aHSC/Myo, which may be targeted through these approaches [34,68]. Future studies will explore the feasibility and efficacy of these next-generation precision targeting platforms.

Acknowledgements

This project is supported in part by grant 1R21AA029741-01 from the NIH/NIAAA, the Robert E. and May R. Wright Foundation Trust, and the James H. Zumberge Faculty Research and Innovation Fund to D.E.F. We thank Qihong Yang, Stephanie Pan and the USC ALPD/C Center for assistance with animal experiments and cell isolation. [16].

References

1. De Smet V, Eysackers N, Merens V, Kazemzadeh Dastjerd M, Halder G. Initiation of hepatic stellate cell activation extends into chronic liver disease. Cell Death Dis. 2021. 12: 1110.
2. Arab JP, Cabrera D, Sehrawat TS, Jalan-Sakrikar N, Verma VK. Hepatic stellate cell activation promotes alcohol-induced steatohepatitis through Igfbp3 and SerpinA12. J Hepatol. 2020. 73: 149-160.
3. Higashi T, Friedman SL, Hoshida Y. Hepatic stellate cells as key target in liver fibrosis. Adv Drug Deliv Rev. 2017. 121: 27-42.
4. Zhang Y, Wu Y, Shen W, Wang B, Yuan X. Crosstalk between NK cells and hepatic stellate cells in liver fibrosis. Mol Med Rep. 2022. 25.
5. Li T, Yang Y, Song H, Li H, Cui A. Activated NK cells kill hepatic stellate cells via p38/PI3K signaling in a TRAIL-involved degranulation manner. J Leukoc Biol. 2019. 105: 695-704.
6. Gao B, Radaeva S. Natural killer and natural killer T cells in liver fibrosis. Biochim Biophys Acta. 2013. 1832: 1061-1069.
7. Radaeva S, Wang L, Radaev S, Jeong WI, Park O. Retinoic acid signaling sensitizes hepatic stellate cells to NK cell killing via upregulation of NK cell activating ligand RAE1. Am J Physiol Gastrointest Liver Physiol. 2007. 293: 809-816.
8. Radaeva S, Sun R, Jaruga B, Nguyen VT, Tian Z. Natural killer cells ameliorate liver fibrosis by killing activated stellate cells in NKG2D-dependent and tumor necrosis factor-related apoptosis-inducing ligand-dependent manners. Gastroenterology. 2006. 130: 435-452.
9. Muhanna N, Abu Tair L, Doron S, Amer J, Azzeh M. Amelioration of hepatic fibrosis by NK cell activation. Gut. 2011. 60: 90-98.
10. Gao B, Radaeva S, Jeong WI. Activation of natural killer cells inhibits liver fibrosis: a novel strategy to treat liver fibrosis. Expert Rev Gastroenterol Hepatol. 2007. 1: 173-180.
11. Anouti A, Mellinger JL. The Changing Epidemiology of Alcohol-Associated Liver Disease: Gender, Race, and Risk Factors. Semin Liver Dis. 2023. 43: 50-59.
12. Mellinger JL. Epidemiology of Alcohol Use and Alcoholic Liver Disease. Clin Liver Dis (Hoboken). 2019. 13: 136-139.
13. Julien J, Ayer T, Bethea ED, Tapper EB, Chhatwal J. Projected prevalence and mortality associated with alcohol-related liver disease in the USA, 2019-40: a modelling study. Lancet Public Health. 2020. 5: 316-323.
14. Tapper EB, Parikh ND. Mortality due to cirrhosis and liver cancer in the United States, 1999-2016: observational study. BMJ. 2018. 362: 2817.
15. Tampaki M, Tsochatzis E, Lekakis V, Cholongitas E. Prevalence, characteristics and outcomes of patients with metabolic and alcohol related/associated liver disease (MetALD): a systematic review and meta-analysis. Metabolism. 2025. 163: 156101.
16. Ciardullo S, Mantovani A, Morieri ML, Muraca E, Invernizzi P. Impact of MASLD and MetALD on clinical outcomes: A meta-analysis of preliminary evidence. Liver Int. 2024. 44: 1762-1767.
17. Huang DQ, Mathurin P, Cortez-Pinto H, Loomba R. Global epidemiology of alcohol-associated cirrhosis and HCC: trends, projections and risk factors. Nat Rev Gastroenterol Hepatol. 2023. 20: 37-49.

18. Vannier AGL, Shay JES, Fomin V, Patel SJ, Schaefer E. Incidence and Progression of Alcohol-Associated Liver Disease After Medical Therapy for Alcohol Use Disorder. JAMA Netw Open. 2022. 5: 2213014.
19. Kamm DR, McCommis KS. Hepatic stellate cells in physiology and pathology. J Physiol. 2022. 600: 1825-1837.
20. Xiong X, Kuang H, Ansari S, Liu T, Gong J. Landscape of Intercellular Crosstalk in Healthy and NASH Liver Revealed by Single-Cell Secretome Gene Analysis. Mol Cell. 2019. 75: 644-660.
21. Gao B, Radaeva S, Park O. Liver natural killer and natural killer T cells: immunobiology and emerging roles in liver diseases. J Leukoc Biol. 2009. 86: 513-528.
22. Jeong WI, Park O, Gao B. Abrogation of the antifibrotic effects of natural killer cells/interferon-gamma contributes to alcohol acceleration of liver fibrosis. Gastro enterology. 2008. 134: 248-258.
23. Little A, Li Y, Zhang F, Zhang H. Chronic alcohol consumption exacerbates murine cytomegalovirus infection via impairing nonspecific and specific NK activation in mice. FASEB Bioadv. 2019. 1: 18-31.
24. Zhang F, Little A, Zhang H. Chronic alcohol consumption inhibits peripheral NK cell development and maturation by decreasing the availability of IL-15. J Leukoc Biol. 2017. 101: 1015-1027.
25. Byun JS, Yi HS. Hepatic Immune Microenvironment in Alcoholic and Nonalcoholic Liver Disease. Biomed Res Int. 2017. 2017: 6862439.
26. Jin S, Shang Z, Wang W, Gu C, Wei Y. Immune Co-inhibitory Receptors CTLA-4, PD-1, TIGIT, LAG-3, and TIM-3 in Upper Tract Urothelial Carcinomas: A Large Cohort Study. J Immunother. 2023. 46: 154-159.
27. Zhao J, Li L, Yin H, Feng X, Lu Q. TIGIT: An emerging immune checkpoint target for immunotherapy in autoimmune disease and cancer. Int Immunopharmacol. 2023. 120: 110358.
28. Mathews S, Xu M, Wang H, Bertola A, Gao B. Animals models of gastrointestinal and liver diseases. Animal models of alcohol-induced liver disease: pathophysiology, translational relevance, and challenges. Am J Physiol Gastrointest Liver Physiol. 2014. 306: 819-823.
29. Bertola A, Mathews S, Ki SH, Wang H, Gao B. Mouse model of chronic and binge ethanol feeding the NIAAA model. Nat Protoc. 2013. 8: 627-637.
30. Hui E, Cheung J, Zhu J, Su X, Taylor MJ. T cell costimulatory receptor CD28 is a primary target for PD-1-mediated inhibition. Science. 2017. 355: 1428-1433.
31. Banta KL, Xu X, Chitre AS, Au-Yeung A, Takahashi C. Mechanistic convergence of the TIGIT and PD-1 inhibitory pathways necessitates co-blockade to optimize anti-tumor CD8. Immunity. 2022. 55: 512-526.
32. Lazaro R, Wu R, Lee S, Zhu NL, Chen CL. Osteopontin deficiency does not prevent but promotes alcoholic neutrophilic hepatitis in mice. Hepatology. 2015. 61: 129-140.
33. Xu J, Chi F, Guo T, Punj V, Lee WN. NOTCH reprograms mitochondrial metabolism for proinflammatory macrophage activation. J Clin Invest. 2015. 125: 1579-1590.
34. Krenkel O, Hundertmark J, Ritz TP, Weiskirchen R, Tacke F. Single Cell RNA SequencingIdentifies Subsets of Hepatic Stellate Cells and Myofibroblasts in Liver Fibrosis. Cells. 2019. 8.
35. Krenkel O, Puengel T, Govaere O, Abdallah AT, Mossanen JC, Kohlhepp M, et al. Therapeutic inhibition of inflammatory monocyte recruitment reduces steatohepatitis and liver fibrosis. Hepatology. 2018;67(4):1270-83.
36. Su Q, Kim SY, Adewale F, Zhou Y, Aldler C. Single-cell RNA transcriptome landscape of hepatocytes and non-parenchymal cells in healthy and NAFLD mouse liver. iscience. 2021. 24: 103233.
37. Yu Z, Xie X, Su X, Lv H, Song S. ATRA-mediated-crosstaIk between stellate cells and Kupffer cells inhibits autophagy and promotes NLRP3 activation in acute liver injury. Cell Signal. 2022. 93: 110304.
38. Matsuda M, Seki E. Hepatic Stellate Cell-Macrophage Crosstalk in Liver Fibrosis and Carcinogenesis. Semin Liver Dis. 2020. 40: 307-320.
39. Yang AY, Wistuba-Hamprecht K, Greten TF, Ruf B. Innate-like T cells in liver disease. Trends Immunol. 2024. 45: 535-548.
40. Li M, Wang L, Cong L, Wong CC, Zhang X. Spatial proteomics of immune microenvironment in nonalcoholic steatohepatitis-associated hepatocellular carcinoma. Hepatology. 2024. 79: 560-574.
41. Peng Y, Wong CC, Yu J. The paradox of immunotherapy in NASH-HCC. Signal Transduct Target Ther. 2021. 6: 228.
42. Ham SD, Abraham MN, Deutschman CS, Taylor MD. Single-cell RNA sequencing reveals Immune Education promotes T cell survival in mice subjected to the cecal ligation and puncture sepsis model. Front Immunol. 2024. 15: 1366955.
43. Song P, Zhang J, Zhang Y, Shu Z, Xu P. Hepatic recruitment of CD11b+Ly6C+inflammatory monocytes promotes hepatic ischemia/reperfusion injury. Int J Mol Med. 2018. 41: 935-945.
44. Ramachandran P, Pellicoro A, Vernon MA, Boulter L, Aucott RL. Differential Ly-6C expression identifies the recruited macrophage phenotype, which orchestrates the regression of murine liver fibrosis. Proc Natl Acad Sci USA. 2012. 109.
45. Liu X, Rosenthal SB, Meshgin N, Baglieri J, Musallam SG. Primary Alcohol-Activated Human and Mouse Hepatic Stellate Cells Share Similarities in Gene-Expression Profiles. Hepatol Commun. 2020. 4: 606-626.
46. Torres S, Abdullah Z, Brol MJ, Hellerbrand C, Fernandez M. Recent Advances in Practical Methods for Liver Cell Biology: A Short Overview. Int J Mol Sci. 2020. 21.
47. Fraietta JA, Lacey SF, Orlando EJ, Pruteanu-Malinici I, Gohil M, Lundh S. Determinants of response and resistance to CD19 chimeric antigen receptor (CAR) T cell therapy of chronic lymphocytic leukemia. Nat Med. 2018. 24: 563-571.
48. Lim WA, June CH. The Principles of Engineering Immune Cells to Treat Cancer. Cell. 2017. 168: 724-740.
49. Maude SL, Laetsch TW, Buechner J, Rives S, Boyer M. Tisagenlecleucel in Children and Young Adults with B-Cell Lymphoblastic Leukemia. N Engl J Med. 2018. 378: 439-448.
50. Kasztelan-Szczerbinska B, Zygo B, Rycyk-Bojarzynska A, Surdacka A, Rolinski J. Blood concentrations of mediators released from activated neutrophils are related to the severity of alcohol-induced liver damage. PLoS One. 2023. 18: 0280068.

51. Kasztelan-Szczerbinska B, Adamczyk K, Surdacka A, Rolinski J, Michalak A. Gender-related disparities in the frequencies of PD-1 and PD-L1 positive peripheral blood T and B lymphocytes in patients with alcohol-related liver disease: a single center pilot study. PeerJ. 2021. 9: 10518.
52. Ma R, Su H, Jiao K, Liu J. Role of Th17 cells, Treg cells, and Th17/Treg imbalance in immune homeostasis disorders in patients with chronic obstructive pulmonary disease. Immun Inflamm Dis. 2023. 11: 784.
53. Kasztelan-Szczerbińska B, Surdacka A, Celiński K, Roliński J, Zwolak A. Prognostic Significance of the Systemic Inflammatory and Immune Balance in Alcoholic Liver Disease with a Focus on Gender-Related Differences. PLoS One. 2015. 10: 0128347.
54. Wu KJ, Qian QF, Zhou JR, Sun DL, Duan YF. Regulatory T cells (Tregs) in liver fibrosis. Cell Death Discov. 2023. 9: 53.
55. Ikeno Y, Ohara D, Takeuchi Y, Watanabe H, Kondoh G. Foxp3+ Regulatory T Cells Inhibit CCI. Front Immunol. 2020. 11: 584048.
56. Wang H, Wu T, Wang Y, Wan X, Qi J. Regulatory T cells suppress excessive lipid accumulation in alcoholic liver disease. J Lipid Res. 2019. 60: 922-936.
57. Koda Y, Nakamoto N, Chu PS, Teratani T, Ueno A, Amiya T. CCR9 axis inhibition enhances hepatic migration of plasmacytoid DCs and protects against liver injury. JCI Insight. 2022. 7.
58. Highton AJ, Schuster IS, Degli-Esposti MA, Altfeld M. The role of natural killer cells in liver inflammation. Semin Immunopathol. 2021. 43:519-533.
59. Markwick LJ, Riva A, Ryan JM, Cooksley H, Palma E. Blockade of PD1 and TIM3 restores innate and adaptive immunity in patients with acute alcoholic hepatitis. Gastroenterology. 2015. 148: 590-602.
60. Lin CT, Wu SJ, Liao CH, Weng RR, Lin CM. The novel CD16A/anti-CD3 bifunctional protein, eCD16A/anti-CD3-BFP, redirects T cell cytotoxicity toward antibody-bound target cells. Hum Vaccin Immunother. 2025. 21: 2447141.
61. Rujirachaivej P, Siriboonpiputtana T, Choomee K, Supimon K, Sangsuwannukul T. Engineered T cells secreting aB7-H3-aCD3 bispecific engagers for enhanced anti-tumor activity against B7-H3 positive multiple myeloma: a novel therapeutic approach. J Transl Med. 2025. 23: 54.
62. Bisio M, Legato L, Fasano F, Benevolo Savelli C, Boccomini C. Bispecific Antibodies for Lymphoid Malignancy Treatment. Cancers (Basel). 2024. 17.
63. Efimov GA, Kruglov AA, Khlopchatnikova ZV, Rozov FN, Mokhonov VV. Cell-type-restricted anti-cytokine therapy: TNF inhibition from one pathogenic source. Proc Natl Acad Sci USA. 2016. 113: 3006-3011.
64. Goulding J, Yeh WI, Hancock B, Blum R, Xu T, Yang BH. A chimeric antigen receptor uniquely recognizing MICA/B stress proteins provides an effective approach to target solid tumors. Med. 2023. 4: 457-477.
65. Daher M, Basar R, Gokdemir E, Baran N, Uprety N. Targeting a cytokine checkpoint enhances the fitness of armored cord blood CAR-NK cells. Blood. 2021. 137: 624-636.
66. Le Saux O, Ray-Coquard I, Labidi-Galy SI. Challenges for immunotherapy for the treatment of platinum resistant ovarian cancer. Semin Cancer Biol. 2020.
67. Liu E, Marin D, Banerjee P, Macapinlac HA, Thompson P. Use of CAR-Transduced Natural Killer Cells in CD19-Positive Lymphoid Tumors. N Engl J Med. 2020. 382: 545-553.
68. Wen Y, Lambrecht J, Ju C, Tacke F. Hepatic macrophages in liver homeostasis and diseases-diversity, plasticity and therapeutic opportunities. Cell Mol Immunol. 2021. 18: 45-56.
69. Mederacke I, Dapito DH, Affò S, Uchinami H, Schwabe RF. High-yield and high-purity isolation of hepatic stellate cells from normal and fibrotic mouse livers. Nat Protoc. 2015. 10: 305-315.